npj | Quantum Information

www.nature.com/npjqi

ARTICLE OPEN

Towards practical quantum metrology with photon counting

Jonathan CF Matthews[1,5], Xiao-Qi Zhou[2,5], Hugo Cable[1,5], Peter J Shadbolt[1,5,6], Dylan J Saunders[3,6], Gabriel A Durkin[4], Geoff J Pryde[3] and Jeremy L O'Brien[1]

Quantum metrology aims to realise new sensors operating at the ultimate limit of precision measurement. However, optical loss, the complexity of proposed metrology schemes and interferometric instability each prevent the realisation of practical quantum-enhanced sensors. To obtain a quantum advantage in interferometry using these capabilities, new schemes are required that tolerate realistic device loss and sample absorption. We show that loss-tolerant quantum metrology is achievable with photon-counting measurements of the generalised multi-photon singlet state, which is readily generated from spontaneous parametric downconversion without any further state engineering. The power of this scheme comes from coherent superpositions, which give rise to rapidly oscillating interference fringes that persist in realistic levels of loss. We have demonstrated the key enabling principles through the four-photon coincidence detection of outcomes that are dominated by the four-photon singlet term of the four-mode downconversion state. Combining state-of-the-art quantum photonics will enable a quantum advantage to be achieved without using post-selection and without any further changes to the approach studied here.

npj Quantum Information (2016) **2,** 16023; doi:10.1038/npjqi.2016.23; published online 9 August 2016

INTRODUCTION

Quantum shot noise represents a hard limit for the precision of all sensors that do not harness quantum resources. Photonic quantum metrology[1] promises to surpass the shot-noise limit (SNL, $\Delta\phi \sim 1/\sqrt{N}$) by using quantum states of light that exhibit entanglement,[2] discord[3] or squeezing[4] to suppress statistical fluctuation in optical-phase estimation. This will ultimately enable greater precision in measuring experimental quantities of interest, such as distance, birefringence, angle or sample concentration. Metrology in the low-photon-flux regime is pursued to gain maximal information while minimising detrimental effects from probe light—for example, in biological sensing.[5,6] This is complementary to the objectives of gravity-wave astronomy schemes that use squeezed light and require high circulating laser power (watts to kilowatts) in km-scale interferometry for sub-SNL performance.[7]

A widespread objective of quantum metrology has been to engineer instances of 'NOON' states,[2,8–12] which are path-entangled states of N photons across two modes $\frac{1}{\sqrt{2}}(|N\rangle|0\rangle + |0\rangle|N\rangle)$. They offer both super-resolution (N-fold decrease in fringe period) and supersensitivity (enhanced precision towards the Heisenberg limit —$\Delta\phi \sim 1/N$), and they are the optimal state for low-flux sensing in the lossless regime. The current record in size of NOON-like states is five photons using post-selection[13] and four photons using ancillary-photon detection.[14] Key components for this architecture have been demonstrated in integrated optics, including state generation and manipulation,[15] micro-fluidics[5] and photon detection.[16] Ultimately, this could enable practical deployment of quantum-enhanced sensors outside of the quantum optics laboratory. However, to date, unavoidable optical loss hampers quantum advantage and can actually lead to worse precision than by just using a bright laser.[2] Moreover, loss will be present in any practical scenario, including absorbance in measured samples and non-unit efficiency detectors. Consequently, revised scaling laws of precision with photon flux have been derived,[17] along with optimised superposition states of fixed photon number, numerically for small photon number[18,19] and analytically for large.[17]

Here, we demonstrate the underpinning principles of a practical —loss-tolerant—scheme for sub-shot-noise interferometry, illustrated in Figure 1. This scheme is designed to use the full four-mode multi-photon state naturally occurring in a non-linear optical process known as type-II spontaneous parametric down-conversion (SPDC), which generates a coherent superposition of correlated photon-number states.[20–22] This scheme can exhibit a remarkably high tolerance to loss by harnessing all detected photon-number correlations arising from the superposition of all generated photon-number components in the generalised singlet state. We greatly simplify the theoretical analysis of a prior version proposed in ref. 23 using the positive-operator-valued measurement (POVM) formalism; this enables application of arbitrary photon-number-counting methods, including the multi-plexed detection scheme used in our experiment here. The scheme can tolerate up to 40% total loss using photon counting without post-selection (Figure 2). To motivate developing such a photon-counting-based system, the type-II SPDC state can be studied in terms of photon-number measurement outcomes in isolation: n-photon detection events can be registered from any

[1]Centre for Quantum Photonics, H.H. Wills Physics Laboratory and Department of Electrical and Electronic Engineering, University of Bristol, Bristol, UK; [2]State Key Laboratory of Optoelectronic Materials and Technologies and School of Physics, Sun Yat-sen University, Guangzhou, China; [3]Centre for Quantum Dynamics and Centre for Quantum Computation and Communication Technology, Griffith University, Brisbane, QLD, Australia and [4]Berkeley Center for Quantum Information and Computation, University of California, Berkeley, CA, USA.
Correspondence: JCF Matthews (Jonathan.Matthews@Bristol.ac.uk) or H Cable (Hugo.Cable@Bristol.ac.uk) or GJ Pryde (G.Pryde@Griffith.edu.au) or JL O'Brien (Jeremy.OBrien@Bristol.ac.uk)
[5]These authors contributed equally to this work.
[6]Current address: Department of Physics, Imperial College London, London, UK.
Received 21 December 2015; revised 5 April 2016; accepted 24 May 2016

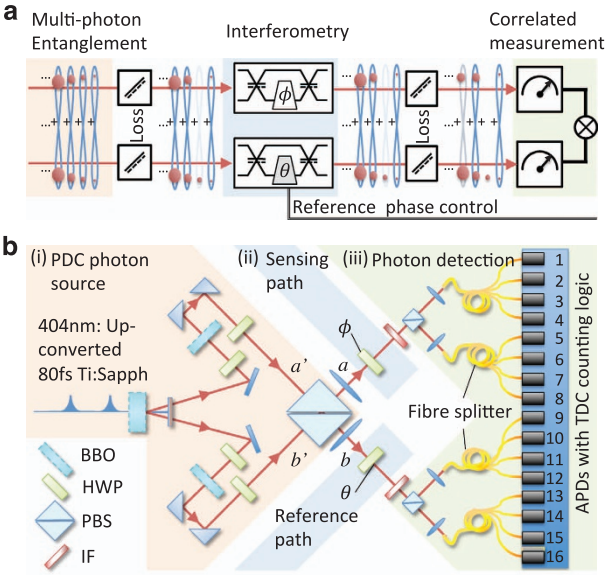

Figure 1. Scheme schematic and our experimental setup. (**a**) Multi-photon entanglement is generated in a form that tolerates loss for quantum-enhanced interferometry. Here, multi-photon entanglement is generated by pulsed type-II PDC, whereas the correlated measurement is performed using photon-counting. (**b**) The probe state $|\mathrm{PDC}\rangle$ of polarisation-entangled photons is generated in a 2 -mm-thick χ^2 non-linear barium borate (BBO) crystal phase matched for non-colinear type-II SPDC.[20] We use a polarising beamsplitter (PBS) to remove spectral-path correlation[43] to ideally generate the desired state $|\mathrm{PDC}\rangle$ across modes (a_h, a_v, b_h, b_v) and spectrally filtered with interference filters (IF). The in-principle unknown phase parameter ϕ and the reference phase θ are implemented using half-waveplates (HWP). θ could be used to shift the interference pattern of ϕ, but we initially use it to zero ϕ.

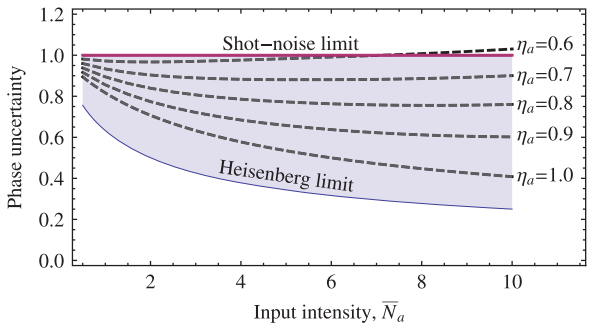

Figure 2. Performance of photon counting and type-II SPDC in the presence of loss $(1-\eta_a)$, without heralding or post-selection. The uncertainty (or error, quantified by the reciprocal of precision) of estimating or detecting an unknown phase ϕ is defined as $\Delta\phi\sqrt{\eta_a\overline{N}_a}$, renormalised by the average intensity $\eta_a\overline{N}_a$ in the interferometer—equivalently one can consider the available statistical information defined as Fisher information per photon. We compare the scheme with the shot-noise limit achieved using perfect coherent laser light, and the Heisenberg limit, $1/\sqrt{\langle\hat{N}_a^2\rangle}$ (relevant to cases in which the total photon number fluctuates[37]). Loss is balanced in the sensing interferometer, and $\overline{N}_a$ is the average number of photons entering the interferometer, before loss.

photon-number component of the entire multi-photon state $\geqslant n$, under all loss. Here, we measure the fourfold detection events arising from all SPDC contributions of four or more photons, which is the smallest non-trivial measurement subset that displays the singlet behaviour with more than one photon in the sensing interferometer of the scheme (and thereby capable of exhibiting quantum advantage). When accounting for all photons passing through the phase shift ϕ in our experiment, the total loss in our experiment of $\sim$83% prohibits us from observing precision that surpasses the SNL. However, as evidence of the potential of this scheme to provide a quantum advantage, we investigate experimentally the correlations of the subset of fourfold detection events, which in principle enable a quantum advantage of up to 45% in the mean-squared error for estimating phase for our measured experimental parameters, and we find that the dynamics we observe is in good agreement with theoretical prediction.

Our approach addresses serious challenges faced by discrete-variable photon-counting schemes that are designed to operate with a deterministically generated or heralded fixed number of photons. The only system that has demonstrated quantum interference of more than two photons is SPDC, and complex experimental techniques comprising optical delay, fast switching and auxiliary photon detection are required to generate fixed photon-number states. This includes approaches to loss-tolerant quantum metrology, such as Holland and Burnett states.[24–27] To perform experiments with n photons, post-selection is commonly used to ignore components of fewer photons ($<n$), whereas terms associated with higher-photon number ($>n$) are treated as noise. This is particularly problematic for quantum metrology, where all photons passing through the sample need to be accounted for, and unwanted photon-number components are detrimental to measurement precision. In contrast, for the scheme presented here, higher-photon terms contribute to enhancement of phase sensitivity of the fourfold detection events.

The Scheme: metrology using type-II SPDC

Our demonstration (Figure 1b) can be treated in three stages: (i) a source of multi-photon entangled light, (ii) unitary rotation with an unknown parameter ϕ to be estimated on the sensing path a, equivalent to interferometry and (iii) correlated photon-counting measurement.

(i) The source is based on pulsed non-colinear type-II SPDC[20,21], which generates entanglement across four modes—two spatial paths (a, b) and two polarisations (h,v) (see Materials and methods). In the ideal case, for which all experimental imperfections are neglected, the state generated is a four-mode squeezed state[23] that is the superposition of photon-number states that are symmetrical across a and b

$$|\mathrm{PDC}\rangle \propto \sum_{n=0}^{\infty} (\tanh\tau)^n \left[\sum_{m=0}^{n} (-1)^m |n-m, m, m, n-m\rangle\right] \quad (1)$$

where τ is an interaction parameter that corresponds to the parametric gain, and the modes are listed in order (a_h, a_v, b_h, b_v). For example, the four-photon term $|2,0,0,2\rangle$ comprises two horizontally polarised photons in path a and two vertically polarised photons in path b. Note that we have omitted normalisation. This state has the property that each term indexed by n corresponds to an entangled state having a total of $2n$ photons, and maps onto the singlet state that represents two spin $-\frac{n}{2}$ systems in the Schwinger representation.[28] When τ is small, as is the case for our experiment with $\tau=0.061$, $|\mathrm{PDC}\rangle$ is dominated by the $n=1$ term, which enables post-selection of the two-photon entangled state[1] $\frac{1}{\sqrt{2}}(|H\rangle_a|V\rangle_b - |V\rangle_a|H\rangle_b)$, which is now common in quantum optics, as ref. 20. For larger τ, the photon intensity grows as $\sim 2\sinh^2\tau$ (ref. 21). The symmetry and correlation properties of $|\mathrm{PDC}\rangle$ have been the subject of several investigations, with experimental evidence reported for entanglement between $\sim$100 photons,[29] with possible applications proposed outside of metrology.[21,30] However, the potential for increasing temporal indistinguishability when using optical

cavities to increase gain τ needs to be considered in future developments of the scheme investigated here.

The four-mode squeezed state (1) that we require is a coherent superposition of multi-photon Fock-state terms; this is distinct to an undesirable statistical mixture of photon pairs. To avoid this mixture in the state generation, it is important to use a pulsed laser pump that has a pulse duration shorter than the coherence length of the photon pairs generated. The detector time bandwidth is longer than the coherence envelope of the generated photons in our experiment. However, with our interference filters (<3 nm bandwidth), we estimate a coherence time of >700 fs, whereas the jitter on the Perkin & Elmer single-photon counting module (SPCM, Excelitas Technologies corp., Waltham, MA, USA) that we use is of the order picosecond. However, the pulses of our pump laser (which we estimate to be <160-fs long, after SHG of 85 fs Ti:sapph) act as an effective gate:[11] the pulses are separated by 12 ns, and our detectors and coincidence logic can resolve well within this window. Temporal modes can introduce large amounts of distinguishability between photons generated in SPDC when the pulse length of the pump laser is longer than the coherence length of the photons generated. This is not the case in our experiment. Evidence that we have achieved this is given by the close agreement between theory and experiment of our multi-photon interference fringes in Figure 3. As highlighted by, for example, ref.11, the quantum interference of statistically mixed photon pairs in different temporal modes differs from that of photon-number Fock states.

(ii) The rotation we consider is

$$U_a(\phi) = \begin{pmatrix} \cos(\phi/2) & \sin(\phi/2) \\ \cos(\phi/2) & -\cos(\phi/2) \end{pmatrix} \quad (2)$$

where ϕ is the parameter we wish to estimate with quantum-enhanced precision. This operator maps exactly to rotations of any two-level quantum system, including the relative phase shift in an interferometer. We implement $U_a(\phi)$ using a half-waveplate in the sensing path a, operating on modes $\{a_h, a_v\}$, for which ϕ is four times the waveplate's rotation angle.

(iii) Finally, photons in each of the four modes (a_h, a_v, b_h, b_v) are detected with number-resolving photodetection—the original proposal[23] assumed fully photon-number-resolving detectors that implement projections onto all Fock states. We approximate number-resolving detection using a multiplexed method[25,31] using readily available components. We use four 1×4 optical fibre splitters with 16 'bucket detector' avalanche photodiode SPCM (APDs). Each APD has two possible outcomes: no detection event ('0') for a vacuum projection and a detection event ('1') for the detection of one or more photons, with nominal $\sim60\%$ efficiency. We use a 16-channel coincidence counting system that records all possible combinations of multi-photon detection events occurring coincidentally across the 16 APDs.

Our approach uses a superposition of all photon-number singlet states and can in principle achieve Heisenberg scaling[23] in a similar manner to NOON states. More importantly, this state surpasses the shot-noise limit despite a realistic level of loss that would otherwise preclude any quantum advantage when using NOON states. The original proposal[23] predicts a quantum advantage in the presence of up to 50% total system loss using a theoretically optimal (but experimentally challenging) measurement scheme, without post-selection. Figure 2 illustrates new results on the sub-SNL performance of photon counting on the Type-II SPDC scheme in the presence of loss. Intuition for the loss tolerance in this scheme can be gained by considering the effect of losing a single photon from one of the modes: each singlet component transforms into a state that closely approximates

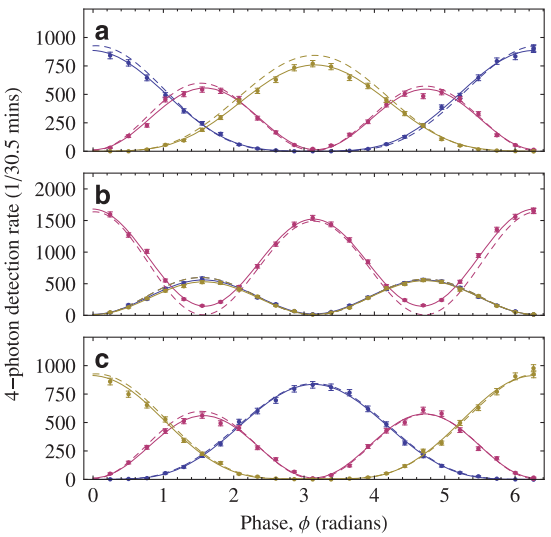

Figure 3. Four-photon interference fringes of $|\mathrm{PDC}\rangle$ in the presence of loss. The detection patterns $r=(r_{ah}, r_{av}, r_{bh}, r_{bv})$ (circular points) correspond to POVM measurements and are as follows: (**a**) 2002 (blue), 2011 (red) and 2020 (gold); (**b**) 1102 (blue), 1111 (red) and 1120 (gold); and (**c**) 0202 (blue), 0211 (red) and 0220 (gold). Note that it is possible to detect bunched photons in the a_h and a_v modes, with rates dependent on the value of ϕ, because of what is effectively two-photon interference in an interferometer.[8] Error bars are computed assuming Poisson-distributed noise on detection statistics. Curves of best fit (solid lines) are computed using functions derived from theory $-\sum_{s=0}^{2} C_s \cos(s(\phi+\phi_o))$, for free parameters C_s and ϕ_o. Theoretical distributions $P_r(\phi)$ (dashed lines) are computed for each r with characterised parameters $\tau=0.061$, $\eta_a=0.23$, $\eta_b=0.12$.

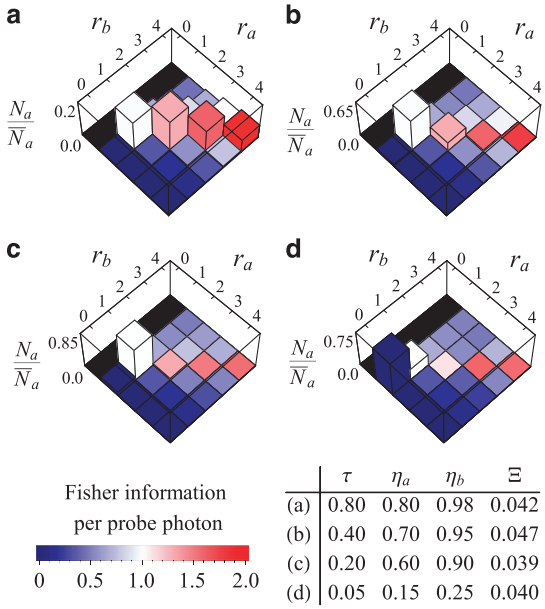

	τ	η_a	η_b	Ξ
(a)	0.80	0.80	0.98	0.042
(b)	0.40	0.70	0.95	0.047
(c)	0.20	0.60	0.90	0.039
(d)	0.05	0.15	0.25	0.040

Figure 4. Illustrative examples of the relationships between Fisher information per probe photon for subsets of detection outcomes having total detection outcomes in each arm (r_a, r_b), and the relative intensity of these outcomes $N_a/\overline{N}_a$ in path a (which sum to 1). The Fisher information per probe photon is plotted as a temperature map (red/white/blue is better than/equal to/worse than the shot-noise limit). Each panel (**a–d**) is for different pump power (τ) and transmittance (η_a, η_b), as shown in the table inset. The effects of loss on $P'(\phi)$ are parameterised by $\Xi=\sqrt{(1-\eta_a)(1-\eta_b)}\tanh\tau$. The outcomes with high-Fisher information highlight the key role played by detection outcomes $r_a=r_b$. The achievable precision exceeds the shot-noise limit without post-selection in the case of **a** where phase uncertainty is improved by 7.6% with intensity in the sensing arm of $\overline{N}_a=1.26$.

another singlet of lower photon number.[21] As loss decreases, detection outcomes of equal photon numbers detected in the sensing and reference arm become the dominant contribution (See Figure 4 and the associated discussion below). Experimentally, we observe sub-SNL phase sensitivity in the four-photon coincidence detection subspace of our experiment, without post-selecting zero loss or assuming a fixed photon number in our theoretical analysis. This supports the loss tolerance expected from detecting $N>4$ from any higher-photon number components of type-II SPDC.[23]

POVM theory

A powerful method to simplify calculating measurement outcome probabilities for our experiment is to use the POVM formalism.[32,33] All photon-counting operations correspond to POVM elements E_r, which are diagonal in the Fock-state basis $\{|c\rangle\}$:

$$E_r = \sum_{c=0}^{\infty} w_r(c)|c\rangle\langle c|, \tag{3}$$

where r and c denote the detection pattern and the photon number, respectively. The weights $w_r(c)$ are non-negative and satisfy $\sum_r w_r(c)=1$. The probability of r detection events is given by $P_r = \mathrm{tr}(\rho\hat{E}_r)$, where ρ is the density matrix of any state input to the measurement setup. For the perfectly number-resolving case, the only non-zero POVM weight is when $c=r$ and $w_r(r)=1$. However, with multiplexed detection, all weights $w_r(c)$ with $c \geqslant r$ can be non-zero. For example, for a two-photon state incident on one of our multiplexed detectors, there is a probability of 1/4 that both photons go to the same APD causing one detection event ($w_1(2)=1/4$) and a probability of 3/4 for two detection events ($w_2(2)=3/4$). The entire table of the POVM weights for our multiplexed system is illustrated in Figure 5. The method to compute these weightings stems from ref. 34 and is explained in the Supplementary Information.

Multiplexed detector POVMs are applied to each of the modes a_h, a_v, b_h and b_v to compute the probability for a detection outcome $r=(r_{ah}, r_{av}, r_{bh}, r_{bv})$, given a phase rotation ϕ:

$$P_r(\phi) = \sum\nolimits_{c_{ah},c_{av},c_{bh},c_{bv}\geq 0} w_{r_{ah}}(c_{ah})w_{r_{av}}(c_{av})w_{r_{bh}}(c_{bh})w_{r_{bv}}(c_{bv})p_c(\phi) \tag{4}$$

where $c=(c_{ah}, c_{av}, c_{bh}, c_{bv})$ is the photon number for each mode and $p_c(\phi)$ corresponds to the probability for a measurement outcome of a perfect projection $|c_{ah}, c_{av}, c_{bh}, c_{bv}\rangle\langle c_{ah}, c_{av}, c_{bh}, c_{bv}|$. From equation (1), rotation on modes a_h and a_v yields the probability to detect c according to

$$p_c = \delta_{c_a,c_b}\frac{\tanh^{2c_a}\tau}{\cosh^4\tau}|\langle c_{ah}, c_{av}|\mathrm{U}(\phi)|c_{bh}, c_{bv}\rangle|^2 \tag{5}$$

where photon number for the two paths is denoted by $c_a=c_{ah}+c_{av}$ and $c_a=c_{bh}+c_{bv}$, and where the Wigner-d matrix element $d^j_{m',m}(\phi)=|\langle j+m', j-m'|U(\phi)|j+m, j-m\rangle|^2$ describes the rotation amplitudes on two separate modes populated by number states,[28] and is conveniently represented as a cosine Fourier series.[23]

We incorporate the total circuit and detector efficiency (η) into the POVM elements via an adjustment of $w_r(c)$. We use a standard loss model for which the mode in question is coupled via a hypothetical beamsplitter to an ancillary mode, initially in the vacuum state, which is traced out at the end. We assume that losses are polarisation independent, and therefore all loss that can arise in our setup commutes with $U_a(\phi)$. We model the single-photon detectors in each multiplexed photon-counting array with the same efficiency η_d, and hence detector loss can be incorporated as a loss channel with efficiency η_d to the combined POVM; this loss commutes with fibre splitters and can be considered as part of the combined system efficiency. The effect of system efficiency η can be incorporated into the multiplexed POVM by the linear transformation:

$$|c\rangle\langle c| \mapsto \sum_{c'=c}^{\infty}\binom{c'}{c}\eta^c(1-\eta)^{c'-c}|c'\rangle\langle c'| \tag{6}$$

The weights $w_r(c)$ are altered correspondingly as illustrated in Figure 5.

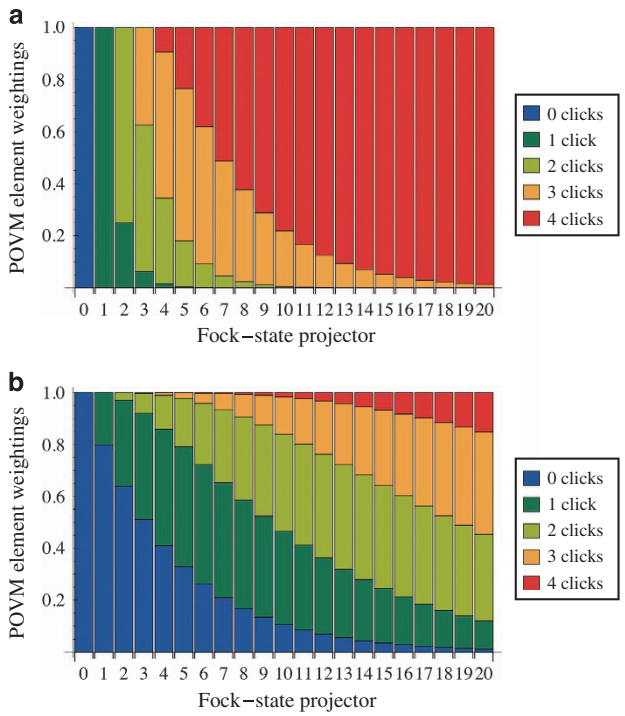

Figure 5. POVM elements for photon counting n using four multiplexed APDs. (**a**) POVM elements with no loss ($\eta=1$). (**b**) Example of the effect on the POVM weightings in the presence of loss ($\eta=0.2$).

RESULTS

In the reported setup, the typical total rates for detecting two photons in coincidence and four photons in coincidence across the two paths are ~17 k per second and ~2 per second, respectively, making our setup suitable for observing sub-SNL precision for the subset of fourfold events. Note that, according to our value of $\tau=0.061$, the rate for the generation of four-photon singlets at the sources is less compared with that for two-photon singlets by a factor $3\tanh^2(0.061)/2\sim 0.006$; however, the measured rates of four- and two-photon coincidences are modified from this because of the effects of losses, as well as limited resolution for the multiplexed photon-number counting for discriminating Fock states $|1\rangle$ and $|2\rangle$.

We plot in Figure 3 all nine possible four-photon detection patterns r of two photons in the reference path and two photons in the sensing path as a function of ϕ, measured simultaneously by the setup in Figure 1b. For comparison, we plot these data together with theoretical curves $P_r(\phi)$, normalising to the total counts collected at each ϕ. These theoretical curves use the measured experimental parameters of $\tau=0.061$, and lumped collection/detection efficiencies of $\eta_a=0.23$ and $\eta_b=0.12$ in the sensing and reference paths, respectively (a geometric average of 83.2% loss), assuming otherwise perfect $U_a(\phi)$ and photon interference. Parameters τ, η_a and η_b are extracted from our setup as follows. The probability of generating one pair of photons

in SPDC is computed via equation (1) and given by

$$p = 2\tanh^2(\tau)/\cosh^4(\tau) \tag{7}$$

We sum the normalised detection rates of pairs of detected single photons that are not part of a coincidence event with $\geqslant 1$ other photon event or with no events elsewhere in the detection scheme:

$$P_{(1,0,0,0)} + P_{(0,1,0,0)} = p\,\eta_b(1-\eta_a) \tag{8}$$

$$P_{(0,0,1,0)} + P_{(0,0,0,1)} = p\,(1-\eta_b)\eta_a \tag{9}$$

Summing all four (normalised) twofold coincidences yields

$$P_{(1,0,0,1)} + P_{(0,1,1,0)} + P_{(1,0,1,0)} + P_{(0,1,0,1)} = p\,\eta_a\eta_b \tag{10}$$

This is then solved for η_b and η_a, then for p, and hence τ via a cubic equation. These relations are assumed to be constant with respect to the phase rotation ϕ and taken as the ϕ-average over experimental data.

The asymmetry in η_a and η_b arises from the different spectral width of the extraordinary and ordinary light on, respectively, paths a and b, passing through identical spectral filtering.[35] The setup is robust to this, as the state symmetry is preserved despite $\eta_a \neq \eta_b$, provided loss is polarisation insensitive.[21] From the data presented in Figure 3, we extract the probability distributions $p_i(\phi)$ as least-square fits from each data set, and normalise such that $\sum_i p_i(\phi) = 1$.

Statistical information about ϕ can be extracted from the frequencies of each output detection pattern and quantified using Fisher information $\mathcal{J}(\phi)$, (ref. 36). We compute the Fisher information of our demonstration using two methods, both plotted in Figure 6. The first (solid black line) is directly computed using the experimentally extracted $p_i(\phi)$ in the relation $\mathcal{J}(\phi) = \sum_{i=1}^{9} p_i(\phi)^{-1}(\mathrm{d}p_i(\phi)/\mathrm{d}\phi)^2$, with error estimated using a Monte-Carlo simulation that assumes Poisson-distributed noise on the four-photon detection rates. The second method is to obtain the variance $\Delta^2\phi_j$ of $\mathcal{M}$ maximum-likelihood estimates $\{\phi_j\}$, each using $\mathcal{N}$ photons, and to evaluate the relation

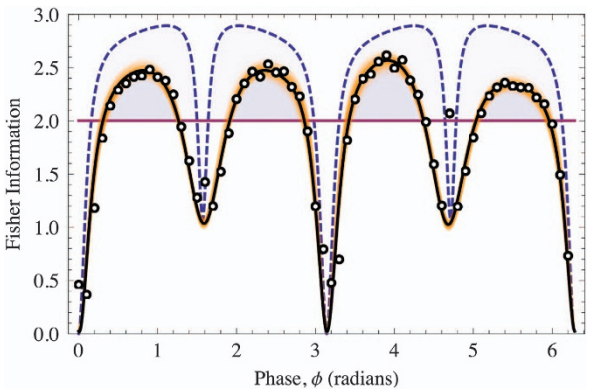

Figure 6. Fisher information extracted from $|\mathrm{PDC}\rangle$ interference fringes. Solid black line: total fisher information $\mathcal{J}(\phi)$ for the fitted probability distributions $p_i(\phi)$ from Figure 3. Orange lines: 1,000 iterations of a Monte-Carlo simulation of $\mathcal{J}(\phi)$, assuming poissonian noise on the raw photon counts. Blue dashed line: Theoretical Fisher information for our setup for ideal four-photon detection patterns computed with the parameters $\tau = 0.061$, $\eta_a = 0.23$, $\eta_b = 0.12$. Purple line: For comparison, the Fisher information for detecting the same intensity as for our experiment in arm a but for classical interferometry. Shaded regions depict where the scheme theoretically and experimentally displays an advantage for the fourfold detection events over detecting the same intensity as for our experiment in arm a but for classical interferometry. Circles: Fisher information $\mathcal{J}_{\mathrm{ML}}(\phi)$ computed from maximum-likelihood estimates of ϕ. Note that $\mathcal{J}_{\mathrm{ML}}(\phi)$ can deviate from $\mathcal{J}(\phi)$, when in close proximity to the edges of the estimation region; we observe this near $\phi = \pi/2$ and $\phi = 3\pi/2$.

$\mathcal{J}_{\mathrm{ML}} = 1/\left(N \times \Delta^2\phi_j\right)$. Note that maximum-likelihood estimation saturates the Cramér–Rao bound and loses any bias as data are accumulated, and it is practical for characterising an unknown phase when $p_i(\phi)$ are characterised. We simulate $\mathcal{M} = 10,000$ maximum-likelihood estimates for a discrete set of waveplate settings, and for each estimate we sample $\mathcal{N} = 1,000$ times from $p_i(\phi)$. This number of samplings ensures unbiased and efficient estimation.[36] Computed values of $\mathcal{J}_{\mathrm{ML}}(\phi)$ are then plotted (circles) in Figure 6, showing close agreement with $\mathcal{J}(\phi)$.

We also plot in Figure 6 theoretical Fisher information computed from the POVM description of our multiplexed detection system, by taking into account the SPDC gain parameter τ and the total circuit and detector efficiency η of our setup. We find general agreement of the main features between theory and experiment ($\mathcal{J}$ and $\mathcal{J}_{\mathrm{ML}}$), whereas the discrepancy is attributed to imperfect waveplate rotations and imperfect indistinguishability (mode overlap) of multi-photon states across the four modes.

Figure 6 also shows the shot-noise limit for two photons passing through the measured phase, computed on the basis of the average photon number in the sensing path for the fourfold detection events. For our experiments $\tau < 0.1$, which bounds the Fisher information for the target path and is computed to lie in the range 2.01 ± 0.01. The shaded region displays the quantum advantage over the shot-noise limit for the post-selected subset of fourfold detection events—the maximum advantage, over detecting the same intensity as for our experiment in arm a but for classical interferometry, achieved in our experiment is $28.2 \pm 2.4\%$ at $\phi = 3.91 \pm 0.06$ rad. The theoretical maximum advantage that can be achieved by the scheme with our τ and η parameters is 45%. This is possible because of the low rate of components with six photons or more compared with four photons for the pre-loss SPDC state (0.5%), and a quantum advantage is predicted theoretically for $\tau \leqslant 0.250$ with our experimental values for loss.

An important feature of the theory and experiment curves in Figure 6 is the troughs in $\mathcal{J}$ (similar features were presented elsewhere, e.g., the Supplementary Information for ref. 25), occurring about points where some or all of the fringes in Figure 3 have minima or maxima. In contrast, when all experimental imperfections are absent, $\mathcal{J}$ is predicted to be independent of phase rotation—a common feature of metrology schemes using photon-number-counting measurement.[37] The definition of $\mathcal{J}(\phi)$ reveals points of instability when the numerator $\mathrm{d}p_i(\phi)/\mathrm{d}\phi$ vanishes but $p_i(\phi)$ does not—this will arise even with very small experiment imperfections that lead to interference fringes with visibility < 1. A solution is to incorporate a reference phase in conjunction with a feedback protocol to optimise the estimation of an unknown phase.[25] The symmetry of the generalised singlet state at the heart of this scheme enables a control phase to be placed on the reference path as opposed to the sensing path in the traditional manner. We demonstrate the feasibility of the former by repeating our experiment with a controllable reference phase rotation (θ in Figure 1b) placed in the reference path b that shifts the regions of maximal sensitivity with respect to the phase in the sensing path—see Supplementary Information for four-photon interference fringes and corresponding Fisher information. This may find practical application where the reference phase has to be separated from the sensing path. Furthermore, the reference path could be used for heralding to maximise the Fisher information per photon passing through the unknown sample using fast switching[38] of the sensing path conditioned on detection events at the reference path. Using heralding and perfect photon-number-resolving detection, the entire downconversion state can achieve quantum advantage with the τ value from our experiment (see Supplementary Information).

Finally, we return to a detailed theoretical analysis of the contribution to phase sensitivity of subsets of outcomes (r_a, r_b).

The symmetry property of $|\mathrm{PDC}\rangle$, namely $U_a \otimes U_b|\mathrm{PDC}\rangle = |\mathrm{PDC}\rangle$ for arbitrary unitary rotation U of polarisation modes, is preserved under polarisation-insensitive photon loss. This maps onto the requirement of polarisation-insensitive loss in our setup—we denote the loss rates in path a (or b) by $1-\eta_{a(b)}$. The symmetry property dictates the general form of the type-II SPDC state post loss, as well as key features of the detection probabilities (after polarisation rotation of a_h, a_v) when outcomes are grouped according to total detections in each arm (r_a, r_b) (refs 21,23). Consequently, we consider renormalised probabilities $P_r^{'}(\phi) = P_r(\phi)/P_{(r_a,\, r_b)}$, where $r = (r_{ah}, r_{av}, r_{bh}, r_{bv})$ and $P_{(r_a,\, r_b)}$ denote the total probability for detections in the subset (r_a,r_b). $P_{(r_a,\, r_b)}$ is independent of the rotation angle when fully number-resolving detectors are used. Only when the total number of photons detected in each of the sensing and reference paths are equal ($r_a = r_b$) does $P_r^{'}(\phi)$ have a singlet contribution (the $n_a = r_a = r_b$ singlet term in equation (1)), whereas all other contributions arise because of loss from singlets with greater photon number (and reduce the achievable precision). The effects of loss on $P_r^{'}(\phi)$ are parameterised by $\Xi = \sqrt{(1-\eta_a)(1-\eta_b)}\tanh\tau$: Ξ increases with higher losses and higher values for τ (which increase the rate of singlet production at high-photon numbers), and it is reduced if the losses are predominantly in one arm. To achieve sub-shot noise precision without post-selection, values of τ and $\eta_{a,b}$ must be chosen to achieve simultaneously a low value of Ξ, high weighting for $P_{(r_a,\, r_b)}$ with $r_a = r_b > 1$ and high average photon number. The components with $r_a = r_b$ provide super-sensitive precision when Ξ is small: this enabling principle of our scheme can be demonstrated using post-selection when high values for τ and $\eta_{a\ (b)}$ are not achieved, as in our current setup. We give illustrative examples in Figure 4.

DISCUSSION

We have demonstrated the key enabling principles of a promising technique for realising practical quantum-enhanced sensors that is robust to loss and designed to use a photon source based on current technology. Our experimental results demonstrate the validity of our theoretical predictions concerning phase super-sensitivity for those detection events that correspond to multi-photon singlet states. Our theory in turn predicts that super-sensitive precision is achievable without post-selection in an experimental regime that is achievable with near-term and state-of-the-art componentry, whereas detection events that have contributions from singlet components behave as in our experiment. Our approach is amenable to near-term implementation in an integrated architecture with on-chip interference of downconversion,[15] on-chip[16] detectors and integration with micro-fluidic channels.[5] This would enable inherently a stable path encoding to measure very small optical path lengths—other bulk optical techniques could be used to achieve this to convert polarisation to path, such as in ref. 39. We note that our scheme does not require optical delays or GHz switching. This is in contrast to other quantum technology schemes that rely on generating a fixed number of photons and therefore require greater architecture complexity—e.g., reliance on heralded photon sources that comprise fast switching, low-loss optical delay, high-speed detection and micro-electronic integration. Our demonstration now shifts the emphasis for practical quantum metrology onto developing and using low-loss circuitry and high-efficiency photon detection; 95% efficiency transition edge sensor[40] and 93% efficient super-conducting nanowire detectors operating in the infrared[41] have recently been reported. For a given efficiency η, the gain parameter τ in the downconversion process also dictates the level of precision the scheme can achieve. As circuit loss is reduced, it would be beneficial to increase τ to the values ($\tau > 1$) studied in ref. 23; enhancing SPDC with a cavity[42] may be a promising approach to achieve this, enabling future experimental work to examine larger photon detection subsets.

MATERIALS AND METHODS

Horizontally polarised 404-nm laser pulses (estimated to be $<$ 160-fs long) are generated by up-conversion (SHG) of a Ti-Sapphire laser system (85 fs pulse length, 80MHz repetition rate). This is focused to a waist of 50 μm within a 2-mm-thick non-linear β barium borate crystal, phase matched for type-II SPDC, to ideally generate the state $|PDC\rangle$ at the intersection of the ordinary (o) and extraordinary (e) cones of photons[20] in paths a' and b' of Figure 1b. Spatial and temporal walk-off between e and o light is compensated[20] with one half-waveplate (optic axis at 45° to the vertical) and one 1 -mm-thick β barium borate crystal in each of the two paths a and b. The spectral width of ordinary and extraordinary light generated in type-II SPDC differs, leading to spectral correlation of the two polarisations. Setting one waveplate to 90° and aligning the two paths onto a PBS separates the e and o light, sending all e light onto output a and all o light onto output b, ref. 43. This removes spectral-path correlation in the PDC state, leaving only polarisation entanglement across paths a and b, and thus erasing polarisation-dependent loss in the sensing path and the reference path of the setup.

ACKNOWLEDGEMENTS

We are grateful for financial support from EPSRC, ERC, NSQI, NRF (SG), MOE (SG) and ARC CQC2T. During the writing of this article, J.C.F.M. was supported by a Leverhulme Trust Early Career Fellowship. X.Z. acknowledges support from University of Bristol, the National Young 1000 Talents Plan and Natural Science Foundation of Guangdong (2016A030312012). G.J.P. acknowledges support from the Benjamin Meaker Visiting Fellowship and from the ARC Future Fellowship. J.L.O'B. acknowledges a Royal Society Wolfson Merit Award and a Royal Academy of Engineering Chair in Emerging Technologies.

COMPETING INTERESTS

The authors declare no conflict of interest.

REFERENCES

1. Giovannetti, V., Lloyd, S. & Maccone, L. Advances in quantum metrology. *Nat. Photon.* **5**, 222 (2011).
2. Dowling, J. P. Quantum optical metrology – the lowdown on high-N00N states. *Contemp. Phys.* **49**, 125 (2008).
3. Modi, K., Cable, H., Williamson, M. & Vedral, V. Quantum Correlations in Mixed-State Metrology. *Phys. Rev. X* **1**, 021022 (2011).
4. Goda, K. *et al.* A quantum-enhanced prototype gravitational-wave detector. *Nat. Phys.* **4**, 472 (2008).
5. Crespi, A. *et al.* Measuring protein concentration with entangled photons. *Appl. Phys. Lett.* **100**, 233704 (2012).
6. Taylor, M. A. *et al.* Biological measurement beyond the quantum limit. *Nat. Photon.* **7**, 229 (2013).
7. The LIGO Scientific Collaboration. A gravitational wave observatory operating beyond the quantum shot-noise limit. *Nat. Phys.* **7**, 962 (2011).
8. Rarity, J. G. *et al.* Two-photon interference in a Mach-Zehnder interferometer. *Phys. Rev. Lett.* **65**, 1348 (1990).
9. Mitchell, M. W., Lundeen, J. S. & Steinberg, A. M. Super-resolving phase measurements with a multiphoton entangled state. *Nature* **429**, 161 (2004).
10. Walther, P. *et al.* De Broglie wavelength of a non-local four-photon state. *Nature* **429**, 158 (2004).
11. Nagata, T., Okamoto, R., O'Brien, J. L., Sasaki, K. & Takeuchi, S. Beating the standard quantum limit with four-entangled photons. *Science* **316**, 726 (2007).
12. Cable, H. & Dowling, J. P. Efficient generation of large number-path entanglement using only linear optics and feed-forward. *Phys. Rev. Lett.* **99**, 163604 (2007).
13. Afek, I., Ambar, O. & Silberberg, Y. High-NOON States by Mixing Quantum and Classical Light. *Science* **328**, 879 (2010).
14. Matthews, J. C. F., Politi, A., Bonneau, D. & O'Brien, J. L. Heralding two-photon and four-photon path entanglement on a chip. *Phys. Rev. Lett.* **107**, 163602 (2011).
15. Silverstone, J. *et al.* On-chip quantum interference between silicon photon-pair sources. *Nat. Photon.* **8**, 104 (2014).
16. Penrice, W. H. O. *et al.* High-speed and high-efficiency travelling wave single-photon detectors embedded in nanophotonic circuits. *Nat. Commun.* **3**, 1325 (2012).

17. Knysh, S., Smelyanskiy, V. N. & Durkin, G. Scaling laws for precision in quantum interferometry and the bifurcation landscape of the optimal state. *Phys. Rev. A* **83**, 021804 (2011).
18. Lee, T.-W. *et al.* Optimization of quantum interferometric metrological sensors in the presence of photon loss. *Phys. Rev. A* **80**, 063803 (2009).
19. Demkowicz-Dobrzanski, R. *et al.* Quantum phase estimation with lossy interferometers. *Phys. Rev. A* **80**, 013825 (2009).
20. Kwiat, P. G. *et al.* New high-intensity source of polarization-entangled photon pairs. *Phys. Rev. Lett.* **75**, 4337 (1995).
21. Lamas-Linares, A., Howell, J. C. & Bouwmeester, D. Stimulated emission of polarization-entangled photons. *Nature* **412**, 887 (2001).
22. Simon, C. & Bouwmeester, D. Theory of an entanglement laser. *Phys. Rev. Lett.* **91**, 053601 (2003).
23. Cable, H. & Durkin, G. Parameter estimation with entangled photons produced by parametric downconversion. *Phys. Rev. Lett.* **105**, 013603 (2010).
24. Holland, M. J. & Burnett, K. Interferometric detection of optical phase shifts at the Heisenberg limit. *Phys. Rev. Lett.* **71**, 1355 (1993).
25. Xiang, G. Y., Higgins, B. L., Berry, D. W., Wiseman, H. M. & Pryde, G. J. Entanglement-enhanced measurement of a completely unknown optical phase. *Nat. Photon.* **5**, 43 (2011).
26. Thomas-Peter, N. *et al.* Real-world quantum sensors: evaluating resources for precision measurement. *Phys. Rev. Lett.* **107**, 113603 (2011).
27. Xiang, G. Y., Hofmann, H. F. & Pryde, G. J. Optimal multi-photon phase sensing with a single interference fringe. *Sci. Rep.* **3**, 2684, (2013).
28. Sakuri, J. J. *Modern Quantum Mechanics* (Addison-Wesley, 1994).
29. Eisenberg, H. S., Khoury, G., Durkin, G. A., Simon, C. & Bouwmeester, D. Quantum entanglement of a large number of photons. *Phys. Rev. Lett.* **93**, 193901 (2004).
30. Radmark, M., Wiesniak, M., Zukowski, M. & Bourennane, M. Experimental filtering of two-, four-, and six-photon singlets from a single parametric down-conversion source. *Phys. Rev. A* **80**, 040302, (R) (2009).
31. Achilles, D. *et al.* Photon-number-resolving detection using time-multiplexing. *J. Mod. Opt.* **51**, 1499 (2004).
32. Peres, A. *Quantum Theory: Concepts and Methods* (Springer, 1993).
33. Kok, P. *et al.* Linear optical quantum computing with photonic qubits. *Rev. Mod. Phys.* **79**, 135 (2007).
34. Sperling, J., Vogel, W. & Agarwal, G. S. True photocounting statistics of multiple on-off detectors. *Phys. Rev. A* **85**, 023820 (2012).
35. Grice, W. P. & Walmsely, I. A. Spectral information and distinguishability in type-II down-conversion with a broadband pump. *Phys. Rev. A* **56**, 1627 (1997).
36. Braunstein, S. L. How large a sample is needed for the maximum likelihood estimator to be approximately Gaussian? *J. Phys. A Math. Gen.* **25**, 3813 (1992).
37. Hoffmann, H. F. All path-symmetric pure states achieve their maximal phase sensitivity in conventional two-path interferometry. *Phys. Rev. A* **79**, 033822 (2009).
38. Bonneau, D. *et al.* Fast Path and Polarization Manipulation of Telecom Wavelength Single Photons in Lithium Niobate Waveguide Devices. *Phys. Rev. Lett.* **108**, 053601 (2012).
39. Jin, X.-M. *et al.* Sequential Path Entanglement for Quantum Metrology. *Sci. Rep.* **3**, 1779 (2013).
40. Lita, A. E., Miller, A. & Nam, S. W. Counting near-infrared single-photons with 95% efficiency. *Opt. Exp.* **16**, 3032 (2008).
41. Marsili, F. *et al.* Detecting single infrared photons with 93% system efficiency. *Nat. Photon.* **7**, 210 (2013).
42. Krischek, R. *et al.* Ultraviolet enhancement cavity for ultrafast nonlinear optics and high-rate multiphoton entanglement experiments. *Nat. Photon.* **4**, 170 (2010).
43. Kim, Y.-H., Kulik, S. P., Chekhova, M. V., Grice, W. P. & Shih, Y. Experimental entanglement concentration and universal Bell-state synthesizer. *Phys. Rev. A* **67**, 010301(R) (2003).

Supplementary Information accompanies the paper on the *npj Quantum Information* website (http://www.nature.com/npjqi)